



Geophysical Research Letters

RESEARCH LETTER

10.1029/2020GL089845

Key Points:

- High-resolution acoustic imaging allows for a detailed analysis of double-diffusive staircases and their finestructure in the Arctic Ocean
- Double-diffusive interface thicknesses and stratifications may be inferred from acoustic observations, providing insight on heat fluxes
- Interface thicknesses appear to be related to water column displacements, and associated stratification changes may be due to turbulence

Supporting Information:

- Supporting Information S1

Correspondence to:

N. C. Shibley,
nicole.shibley@yale.edu

Citation:

Shibley, N. C., Timmermans, M.-L., & Stranne, C. (2020). Analysis of acoustic observations of double-diffusive finestructure in the Arctic Ocean. *Geophysical Research Letters*, 47, e2020GL089845. <https://doi.org/10.1029/2020GL089845>

Received 16 JUL 2020

Accepted 1 SEP 2020

Accepted article online 9 SEP 2020

Analysis of Acoustic Observations of Double-Diffusive Finestructure in the Arctic Ocean

Nicole C. Shibley¹ , Mary-Louise Timmermans¹ , and Christian Stranne² 

¹Department of Earth and Planetary Sciences, Yale University, New Haven, CT, USA, ²Department of Geological Sciences, Stockholm University, Stockholm, Sweden

Abstract Double-diffusive convection may occur if both temperature and salinity increase with depth, as in the Arctic Ocean. The process is identifiable by a staircase structure, with mixed layers separated by high-gradient interfaces in temperature and salinity. These staircases, which persist if turbulence levels are weak, are widely present in the Arctic Ocean and responsible for transporting heat toward the overlying sea ice. Acoustic observations (reflection coefficients) from a broadband echo sounder are analyzed here to track the detailed evolution of interfaces in the Arctic's double-diffusive staircase. We infer interface thicknesses from reflection coefficient profiles and find that thicknesses appear to be related to water column displacements. Further, we relate reflection coefficients to interface stratification and interpret stratification changes in the context of turbulence acting to thicken interfaces. The high-resolution capabilities of the echo sounder allow for insights into how double-diffusive heat fluxes and inferred mixing levels may vary in space/time.

Plain Language Summary Heat contained in the Arctic Ocean influences the overlying sea ice cover and Arctic climate. One important mode of ocean heat transport is double-diffusive convection, which may occur when both temperature and salinity increase with depth. Double-diffusive convection manifests as distinct layered structures (staircases), which are prominent throughout the Arctic Ocean. Here, we use a time series of acoustic measurements with high temporal and spatial resolution to track a double-diffusive staircase. The high-resolution acoustic data allow for an investigation of real-time changes in double-diffusive features, which are then related to larger-scale water column motions. These results shed light on the processes affecting the evolution of double-diffusive staircases and heat transport in a warming Arctic Ocean.

1. Introduction

As the Arctic Ocean warms, understanding the mechanisms by which ocean heat is mixed upwards is crucial to predicting the fate of the overlying sea ice (e.g., Carmack et al., 2015; Kwok & Untersteiner, 2011). In the interior Arctic Ocean, mixing levels are generally low (e.g., Chanona et al., 2018; D'Asaro & Morison, 1992) and associated vertical heat fluxes are weak (e.g., Guthrie et al., 2015; Toole et al., 2010). However, there is enough heat stored in subsurface Arctic waters to melt the overlying Arctic sea ice if this heat were to reach the surface (Maykut & Untersteiner, 1971). In recent years, this relatively warm and salty water layer (*Atlantic Water* sourced from the North Atlantic) has become warmer and the stratification at the top of the layer has weakened (e.g., Polyakov et al., 2017). The implications of these changes to the processes affecting vertical heat transport throughout the Arctic Basin are not fully understood.

An important mechanism for vertical heat transport from the Arctic Ocean's Atlantic Water is double-diffusive convection (e.g., Guthrie et al., 2015; Neal et al., 1969; Padman & Dillon, 1987; Polyakov et al., 2012; Shibley et al., 2017; Timmermans et al., 2008). This mode of heat transport, hereafter diffusive convection, may occur when temperature and salinity increase with depth (e.g., Radko, 2013; Schmitt, 1994; Turner, 1965, 1968) and is found in the Arctic Ocean where the Atlantic Water underlies cooler, fresher water (Figures 1a and 1b). The diffusive-convective process manifests as a staircase structure, with thick mixed layers separated by thinner interfaces in temperature and salinity (Figure 1b). Diffusive-convective heat fluxes through the Atlantic Water staircase range from $O(0.01\text{--}0.1) \text{ W m}^{-2}$ in the interior Arctic basins (e.g., Flanagan et al., 2013; Guthrie et al., 2015; Padman & Dillon, 1987; Shibley et al., 2017; Timmermans et al., 2008) to $O(1) \text{ W m}^{-2}$ around the peripheries (e.g., Polyakov et al., 2012).

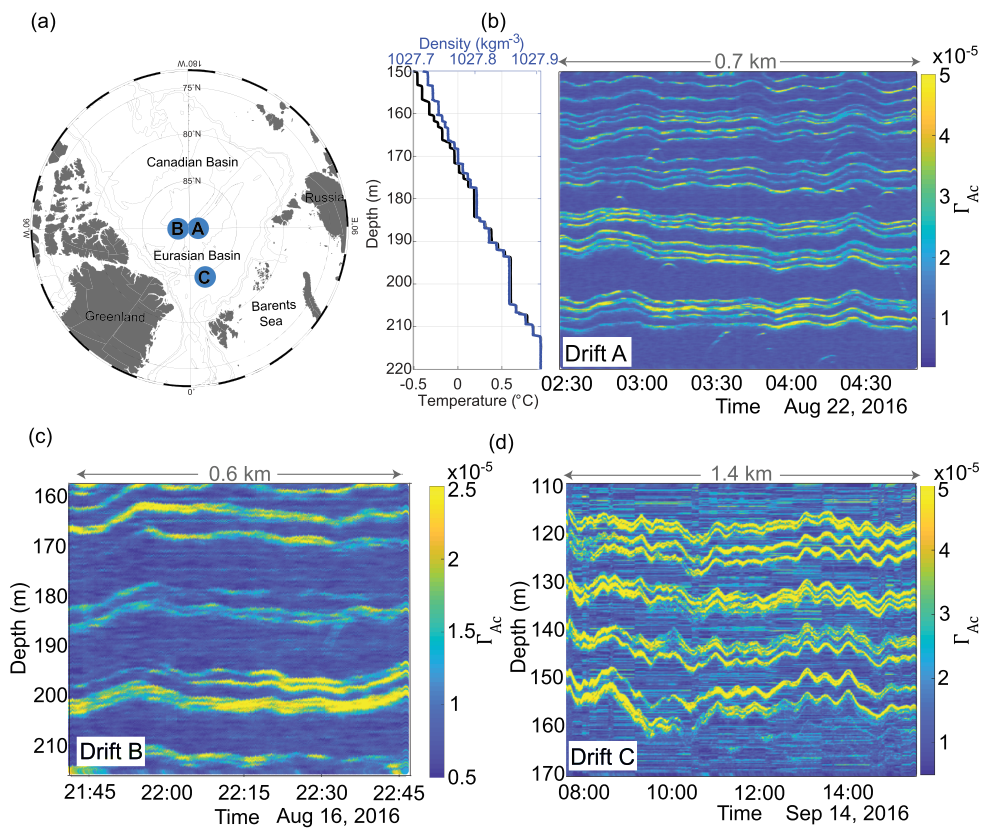


Figure 1. (a) Drift locations of the *Oden* in August–September 2016. Drift A is located at (89.7°N, 52.1°E), Drift B at (89.3°N, 70.2°W), and Drift C at (84.4°N, 17.4°E), with GPS coordinates given at the midpoint of the time series. (b) Echogram at Drift A, spanning 2 hr, 20 min, and 0.7 km. The inset shows the colocated CTD temperature and density profiles at hour 2:40. (c) Echogram at Drift B, spanning 1 hr, 5 min, and 0.6 km. (d) Echogram at Drift C, spanning 7 hr, 51 min, and 1.4 km.

Observations from microstructure profilers or Ice-Tethered Profilers (ITPs, Krishfield et al., 2008) and theory suggest that staircases may not form above a critical level of turbulence (Guthrie et al., 2017; Rippeth et al., 2015; Shibley & Timmermans, 2019), although the exact nature of staircase persistence is not well understood. While the staircase finestructure may be resolved by microstructure measurements, microstructure surveys consist of individual water column profiles spaced by hours and kilometers and cannot capture staircase variability on shorter scales (Fer et al., 2010; Lenn et al., 2011). Further, while ITPs have been effective at tracing staircase properties for hundreds of kilometers (Timmermans et al., 2008), they are limited by a vertical resolution of ~ 25 cm and cannot resolve processes at subhourly and subkilometer horizontal scales. Acoustic imaging techniques provide a more complete view of ocean finestructure and turbulent processes (e.g., Holbrook & Fer, 2005; Holbrook et al., 2003; Lavery et al., 2010; Ross & Lueck, 2003; Stranne et al., 2017). Here we demonstrate that acoustic techniques provide an effective means of observing the staircase finestructure and inferring stratification changes across interfaces on temporal scales of minutes.

1.1. Acoustic Imaging

Acoustic imaging is based on the principle that sound waves sent into the ocean reflect off differences in density or sound speed. Specifically, sound waves are reflected due to differences in impedance $\eta = \rho c$, where $c = \sqrt{K/\rho}$ is the sound speed of water, ρ is the density of water, and K is the bulk modulus. Sounding devices transmit acoustic waves into the ocean, which when reflected off impedance differences, give a measure of the backscatter (target) strength (e.g., Lurton, 2002).

Target strength (γ) is a measure of the relative power of the reflected wave over the area A swept out by the sounding device to the power of the incident wave over an area of 1 m^2 . An acoustic reflection coefficient (Γ_{Ac}) can be inferred from measurements of target strength as $\Gamma_{Ac} = 10^{(\gamma - 10\log_{10}A)/20}$ (e.g., Lurton, 2002; Stranne et al., 2017). With values of ρ and c (inferred from CTD measurements), a reflection coefficient can also be calculated directly at a particular depth i as follows:

$$\Gamma_i = \frac{\eta_i - \eta_{i-1}}{\eta_i + \eta_{i-1}}, \quad (1)$$

where Γ_i is the reflection coefficient at the i th depth (e.g., Lurton, 2002; Stranne et al., 2017).

Acoustic methods to image ocean stratification came to the forefront in the early 2000s when methods used for seismic imaging were applied to the ocean to locate pycnoclines (e.g., Holbrook et al., 2003; Nakamura et al., 2006; Ruddick et al., 2009) and have been used to determine ocean mixing and dissipation rates (Fortin et al., 2016, 2017; Holbrook et al., 2013). Capable of resolving finer details than seismic methods, broadband echo sounders have also been used to image the ocean (Lavery et al., 2010; Lurton, 2002; Stranne et al., 2017, 2018). These echo sounders send out sound pulses with multiple frequencies of O (10–100) kHz, yielding vertical range resolutions of O(1–10) cm, which are sufficiently small to distinguish water column finestructure (Lavery & Ross, 2007; Lavery et al., 2009; Stranne et al., 2017).

Here, we analyze 15–25 kHz echo sounder data, published by Stranne et al. (2017), to assess the capabilities and limitations of echo sounder data in an analysis of the Arctic staircase. In the next section, we describe the echograms (acoustic images of the water column in depth and time) and show how sequential reflection coefficient profiles allow for the tracking of diffusive-convective interfaces and estimates of their thicknesses over time. We then derive an analytical relationship between reflection coefficient and stratification and demonstrate its validity for inferring interface stratifications from echo sounder data. Next the inferred interface thicknesses are analyzed and related to water column motions and vertical displacements. Finally, we use our stratification approximation together with thicknesses to speculate on short-timescale variability in mixing levels and heat fluxes at diffusive-convective interfaces.

2. Echogram Data

Backscatter data (target strengths converted to reflection coefficients) were collected from a Simrad EK80 broadband echo sounder mounted on the icebreaker *Oden* from August–September 2016. We consider portions of three *Oden* drifts in the Eurasian Basin: Drift A (0.7 km drift in 2 hr, 20 min), Drift B (0.6 km drift in 1 hr, 5 min), and Drift C (1.4 km drift in 7 hr, 51 min), Figure 1. Over these small horizontal scales, synoptic features of the Arctic Ocean, generally O(100) km, do not influence the local flow field; variability can be assumed to be effectively temporal.

The time step/ping rate between reflection coefficient profiles is ~10 s. The vertical resolution, based on the speed of sound and the frequency of measurements received by the echo sounder, is ~6 cm (see supporting information, SI). This differs from the range resolution (the minimum vertical distance separating interfaces to be able to distinguish between them), which is about 10 cm. Data processing details are given by Stranne et al. (2017). Each echogram is associated with a colocated CTD profile (bin-averaged every 10 cm, sufficient for validation of diffusive-convective finestructure) taken with a Seabird 911 CTD.

In the echograms, the staircase can be identified by thick layers of lower reflection coefficient separated by thin interfaces of higher reflection coefficient. These changes in reflection coefficient correspond to jumps in impedance η across the interfaces. We consider the following depth ranges spanning the staircase: 150 to 220 m for Drift A, 159 to 215 m for Drift B, and 110 to 170 m for Drift C (Figure 1).

Any acoustic signal may be influenced by noise. To assess noise levels, we examine *rms* run lengths of representative reflection coefficient profiles (neglecting points likely associated with real peaks), which provide a measure of how many consecutive data points fall on either side of the mean value of the signal (e.g., Galbraith & Kelley, 1996); short run lengths imply a noisy signal. For effective analysis of staircase properties, we consider only echograms characterized by run lengths ≥ 10 , where this value was chosen as the threshold above which each individual peak in the corresponding CTD profile could be associated with a peak in the acoustic data. This criterion was satisfied for Drifts A and B, while Drift C had run lengths shorter than

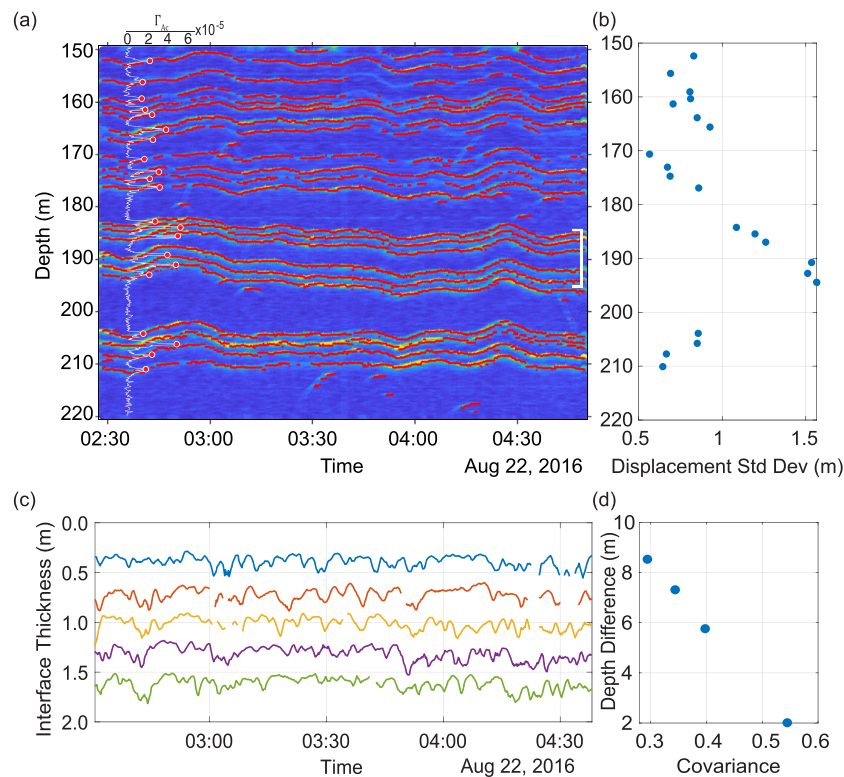


Figure 2. (a) Time series of tracked interfaces (red dots) in depth from Drift A with peaks (circled red dots) chosen in a profile of Γ_{Ac} -depth. (b) Standard deviation of time-averaged vertical displacements (m) for each interface (tracked in panel a) plotted at the mean depth of the interface. (c) Time series of a 1-min moving average of inferred interface thicknesses (Δz) across Drift A for the interfaces bounded by the white bracket on panel a. Each interface is offset from the next by 0.3 m. (d) Covariance of the interfaces shown in panel (c) (from the shallowest—blue line to the fourth shallowest—purple line) with the deepest interface (green line).

this threshold. Higher noise levels in Drift C appear in the echogram as deviations to higher Γ_{Ac} between interfaces (Figure 1d), possibly due to a shorter acoustic pulse length, associated with a lower signal to noise ratio (Stranne et al., 2018). For this reason, our analysis of the echogram data considers only Drifts A and B.

In order to analyze how the layers and interfaces of a staircase evolve, we implement an interface tracking algorithm based on selecting the peak reflection coefficient of each interface at each time step (Figure 2a; see SI). Interface tracking allows for an understanding of the temporal evolution of both water column displacements (Figure 2b) and interface thicknesses, which we infer by fitting Gaussian profiles to reflection coefficient data (Figure 2c; see SI). Further, the peak reflection coefficient at each interface may be used to infer interface stratification via an analytical relationship.

3. Results

3.1. Relating Reflection Coefficient to Stratification

From Equation 1, we formulate an analytical approximation relating reflection coefficient and stratification, $N^2 = (g/\rho_0)(\partial\rho/\partial z)$ (z is depth, and ρ_0 is a reference density). Using $\eta = \rho c$ and expanding Equation 1 as a Taylor series yields

$$\Gamma_i = \frac{(\rho_{i-1} + \frac{\partial\rho}{\partial z}\Big|_{z_{i-1}}\delta z + \dots)(c_{i-1} + \frac{\partial c}{\partial z}\Big|_{z_{i-1}}\delta z + \dots) - \rho_{i-1}c_{i-1}}{(\rho_{i-1} + \frac{\partial\rho}{\partial z}\Big|_{z_{i-1}}\delta z + \dots)(c_{i-1} + \frac{\partial c}{\partial z}\Big|_{z_{i-1}}\delta z + \dots) + \rho_{i-1}c_{i-1}}. \quad (2)$$

ρ_i , ρ_{i-1} and c_i , c_{i-1} are the density and sound speed at depths z_i and z_{i-1} , respectively. The magnitude of Γ_i depends on the spacing between z_i and z_{i-1} (hereafter δz , the measurement resolution, Figure 3a). Neglecting higher-order terms, this is approximated as

$$\Gamma_i \approx \frac{\rho_{i-1} \frac{\partial c}{\partial z} \Big|_{z_{i-1}} + c_{i-1} \frac{\partial \rho}{\partial z} \Big|_{z_{i-1}}}{2\rho_{i-1} c_{i-1}} \delta z, \quad (3)$$

where, based on inspection of the CTD profiles, we take $\frac{\partial \rho}{\partial z} \Big|_{z_{i-1}} \ll \frac{2\rho_{i-1}}{\delta z}$ and $\frac{\partial c}{\partial z} \Big|_{z_{i-1}} \ll \frac{2c_{i-1}}{\delta z}$. The CTD data further indicate that $\frac{1}{c_{i-1}} \frac{\partial c}{\partial z} \Big|_{z_{i-1}}$ is one order of magnitude larger than $\frac{1}{\rho_{i-1}} \frac{\partial \rho}{\partial z} \Big|_{z_{i-1}}$; Γ_i can be approximated as follows:

$$\Gamma_i \approx \frac{\delta z}{2c_{i-1}} \frac{\partial c}{\partial z} \Big|_{z_{i-1}}. \quad (4)$$

Finally, the speed of sound in seawater over the region of interest is approximated as $c \approx a_0 + (a_1 \alpha T + a_2 \beta S + a_3 z)$, where $a_0 = 1,424.30 \text{ m s}^{-1}$, $a_1 = 7.38 \times 10^4 \text{ m s}^{-1}$, $a_2 = 1.79 \times 10^3 \text{ m s}^{-1}$, $a_3 = 0.017 \text{ s}^{-1}$, β is the coefficient of haline contraction, and α is the coefficient of thermal expansion (modified from Wilson, 1959, 1960). We take α and β to be constant over the respective depth ranges, since they vary by <18% and <1%, respectively. The vertical gradient of c is dominated by temperature and salinity terms, with the pressure effect (quantified by a_3) being at least an order of magnitude smaller. Using this approximation for c in Equation 4, and neglecting pressure effects, yields an approximation for the reflection coefficient inferred from CTD data:

$$\tilde{\Gamma}_i = \frac{\delta z}{2c_{i-1}} \left[\alpha \frac{\partial T}{\partial z} (a_1 + a_2 R_\rho) \right], \quad (5)$$

where the density ratio $R_\rho = (\beta \partial S / \partial z) / (\alpha \partial T / \partial z)$ and $\partial S / \partial z$ and $\partial T / \partial z$ are the vertical salinity and temperature gradients, respectively, over the region of interest. Thus, the peak value of $\tilde{\Gamma}_i$ occurs at each interface where $\partial T / \partial z$ is largest, the interface “core” (Figure 3a).

Using a linear approximation for the seawater equation of state $\rho \approx \rho_0(1 - \alpha T + \beta S)$ yields the following approximation for stratification:

$$N^2 \approx -g \alpha \frac{\partial T}{\partial z} (1 - R_\rho). \quad (6)$$

Together with Equation 5, we may write

$$\tilde{N}^2 = -g(1 - R_\rho) \frac{2c_{i-1} \tilde{\Gamma}_i}{\delta z (a_1 + a_2 R_\rho)}, \quad (7)$$

where we refer to the resulting stratification approximation as \tilde{N}^2 . The values of R_ρ and c_{i-1} are chosen for each interface from the colocated CTD for each drift; these values are then taken to be constant across the full time series of each drift. This is appropriate given the short length/time scales, with the caveat that no interface splitting or merging may occur to cause changes in R_ρ (Kelley, 1987, 1988; Radko, 2007; Radko et al., 2014).

Considering acoustic reflection coefficient profiles coincident with CTD profiles, a comparison of peak Γ_{Ac} at each interface with peak $\tilde{\Gamma}_i$ (inferred from the CTD profile using $\delta z = 0.10 \text{ m}$ in Equation 5, for the vertical resolution of the CTD data) indicates good agreement (Figures 3a and 3b). Further, comparing \tilde{N}^2 (using $\delta z = 0.06 \text{ m}$ in Equation 7, the vertical resolution of acoustic profiles) with N^2 inferred directly from CTD measurements yields an almost 1:1 relationship, with an r^2 value of 0.70 (Figure 3c). Thus, it is reasonable to infer stratification across individual interfaces identified in the acoustic data using Equation 7 with Γ_{Ac} replacing

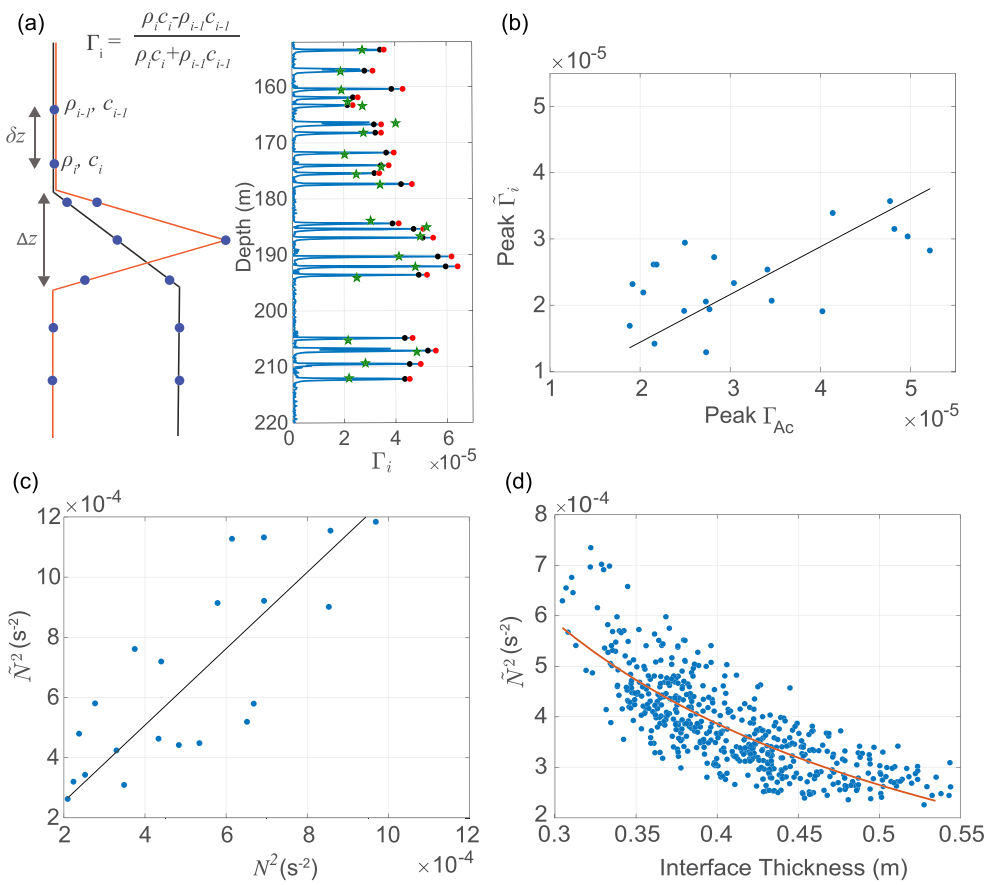


Figure 3. (a) Schematic of an interface (in black) with jumps in density ρ and sound speed c , and measurement resolution δz , and the derived reflection coefficient profile in red (left). A reflection coefficient-depth profile from colocated CTD data at Drift A (right). Red dots indicate peaks exhibited by the data. Black dots show the approximation $\tilde{\Gamma}_i$ estimated from Equation 5. Green stars show peak reflection coefficient inferred from echo sounder data (Γ_{Ac}), offset by 0.8 m to match the CTD depth levels. (b) Peak acoustic reflection coefficient Γ_{Ac} at Drift A for the acoustic reflection coefficient profile corresponding to the colocated CTD profile (with Peak $\tilde{\Gamma}_i$). Peak $\tilde{\Gamma}_i = (0.72 \pm 0.04)\Gamma_{Ac}$, with an r^2 value of 0.59. (c) CTD stratification N^2 compared to estimated stratification \tilde{N}^2 from acoustic reflection coefficients (following Equation 7). $\tilde{N}^2 = (1.27 \pm 0.07)N^2$, with an r^2 value of 0.70. (d) Inferred stratification from acoustic data (\tilde{N}^2) compared to inferred acoustic interface thickness (Δz) from the seventh shallowest interface (at ≈ 167 m) in Drift A ($\tilde{N}^2 = 2.4 \times 10^{-4}/\Delta z - 2.2 \times 10^{-4}$).

$\tilde{\Gamma}_i$. Therefore, if one has continuous echo sounder measurements of peak Γ_{Ac} at an interface and a single CTD profile for values of c_{i-1} and R_ρ , \tilde{N}^2 may be determined for an entire time series evolution of an interface. We next analyze the evolution of thicknesses tracked in the acoustic data and relate this to \tilde{N}^2 .

3.2. Interface Thicknesses and Water Column Motions

The high resolution of the acoustic data allows for an examination of the detailed evolution of interface thicknesses in the staircase (on time scales as small as minutes) that is not possible by traditional sampling. Further, interfaces as thin as about 24 cm can be resolved (see SI). Since these interface thicknesses are inferred from Gaussian fits to the reflection coefficient data, changes in interface thickness of only a few centimeters can be inferred between adjacent time steps. Interface thicknesses vary between approximately 0.3 and 0.7 m over the full transects for both Drifts A and B, with median values of ~ 0.4 m (Figure 4a). The median interface thickness inferred from acoustic data in Drifts A and B is thinner than the minimum interface thickness (0.5 m) able to be resolved with ITPs, confirming that the ITP vertical resolution is a significant limitation (see also Guthrie et al., 2015).

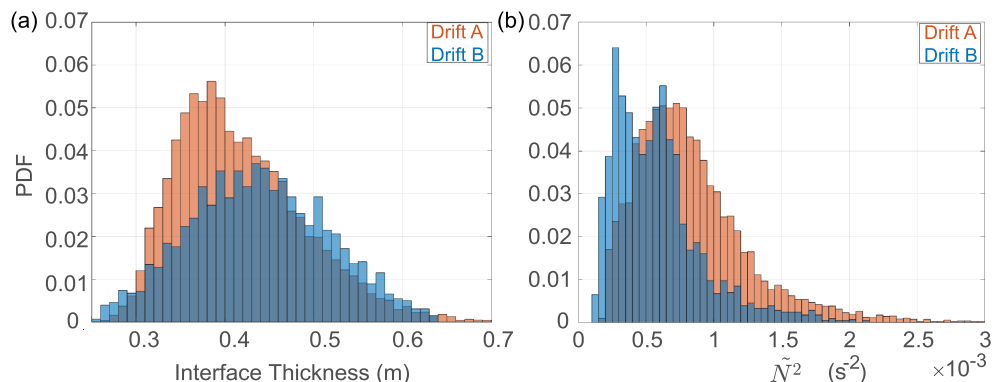


Figure 4. Histograms of (a) interface thickness (Drift A median = 0.41 m, Drift B median = 0.44 m) and (b) interface stratification (Drift A median = $7.5 \times 10^{-4} s^{-2}$, Drift B median = $5.4 \times 10^{-4} s^{-2}$) from all interfaces in Drifts A (orange) and B (blue).

To examine what drives these variations in interface thickness, we begin with the hypothesis that water column heaving, such as that associated with a passing internal wave, may lead to localized mixing at interfaces affecting interface thickness and stratification. Our interface tracking algorithm provides a depth time series for every interface (Figure 2a), yielding a measure of vertical displacements of the water column. We consider the depth region of 180–200 m from Drift A that exhibits relatively large vertical water column displacements (Figure 2b). The displacements (smoothed with a 1-min moving average) of five interfaces spanning that depth are compared against each respective interface thickness time series (Figure 2c). In this depth range, there appears to be a relationship between interface displacement and thickness, with a thickening of interfaces lagging water column displacements. The value of the lag with the highest covariance (0.48) is 27 min, similar for each of the 3 deepest interfaces shown in Figure 2c. The precise mechanism by which this occurs, and a physical explanation for the time lag, is unclear and merits future study with additional observations. The shallowest interface exhibits only a weak maximum covariance (0.20). For the three deepest interfaces for which displacements and interface thicknesses covary strongly, vertical water column velocities (estimated from displacements) of around $0.01 m s^{-1}$ relate to interface thickness increases of around 1 cm.

The same group of five interfaces tends to exhibit similar fluctuations in thickness with time, with the magnitude of covariance being strongest for interfaces that are in closest proximity (Figure 2d). This provides further evidence that coherent vertical displacements influence the group similarly. There is a sixth interface, the deepest, in the same group (Figure 2a) that does not covary in thickness with the others, possibly because it is adjacent to a thick, convecting layer whose large eddies may scour and strain the interface in a manner independent of water column heaving. Correspondence between water column heaving and interface thickness is not apparent in other parts of the water column, where vertical displacements may be too small to influence interface thicknesses above the noise level. Nevertheless, the sample analyzed here suggests that the evolution of interface thickness may be at least partially driven by water column dynamics, leading to possible mixing and changes in stratification.

3.3. Interface Stratification and Interface Diffusivity Estimates

Interface stratification, inferred from Equation 7 with Γ_{Ac} replacing $\tilde{\Gamma}_i$, varies by an order of magnitude from $O(10^{-4})$ to $O(10^{-3}) s^{-2}$ across Drifts A and B (Figure 4b). Values from Drift B tend to be smaller than values from Drift A (a median of $5.4 \times 10^{-4} s^{-2}$ compared to $7.5 \times 10^{-4} s^{-2}$). Changes in stratification are likely due to changes in interface thickness; Γ_{Ac} exhibits a strong covariance (-0.60 on average) with Δz inferred from Gaussian profiles, with deviations to larger Γ_{Ac} corresponding to smaller Δz . Further, stratification estimates inferred from Γ_{Ac} via Equation 7 for a single representative interface sampled in Drift A compared to the corresponding Δz suggest that stratification is inversely proportional to Δz ; over the scales considered here, changes in \tilde{N}^2 across interfaces approximately represent changes in interface thickness. Interface thickening is due to either intermittent turbulence centered on an interface or conductive growth of an interface (when

diffusive-convective fluxes become weak). Over a $\delta t = 3$ min interval, an interface may thicken by conduction by up to $2\sqrt{\kappa_T \delta t} \approx 1$ cm, where $\kappa_T = 1.4 \times 10^{-7}$ m² s⁻¹ is the molecular diffusivity of heat. Interface thickness changes observed in Drifts A and B are several times larger than could be explained by conductive growth alone; we deduce that changes are likely due to intermittent turbulent eddies thickening interfaces. Finally, there appear to be instances where an interface becomes sufficiently weakly stratified that it is not picked up by the interface tracking algorithm. These disappearances last for O(1–10) min and occur only a few times per drift. Over these events, stratification generally decreases prior to the loss of imaging of the interface, consistent with the idea that this may be due to thickening by turbulent eddies.

Under the expectation that intermittent turbulence (shear localized at interfaces) acts to thicken interfaces, we investigate the related mixing (turbulent diffusivity κ at an interface). If interface thickness changes are caused by turbulent eddies, interface κ may be related to interface stratification via Thorpe scales. The Thorpe scale (L_T) describes the *rms* length that water parcels in an unstable density profile would need to be resorted to achieve a stable density profile (Thorpe, 1977). An approximation for κ , from a scaling law relating diffusivity to stratification, yields $\kappa = 0.1NL_T^2$, where N is local stratification (Dillon, 1982; Thorpe, 1977). To determine an appropriate length scale for L_T , we consider the structure of a diffusive-convective interface. An interface is generally assumed to consist of a stable inner core, with unstable density boundary layers on either side (e.g., Carpenter et al., 2012; Shibley & Timmermans, 2019; Linden & Shirtcliffe, 1978). We assume that the stable core is approximately one-third of the thickness of the entire interface, consistent with direct numerical simulations (Carpenter et al., 2012). Assuming that a turbulent overturn occupies only the interface core, we estimate a corresponding κ using $N = \tilde{N}$ and $L_T = \Delta z/3$ (from 8 to 25 cm) to be O(10^{-5}) m² s⁻¹. It is possible that the length scales of intermittent turbulence operating at an interface are actually smaller than our estimates for the interface core thickness, which may reduce the estimated values of κ .

Past microstructure surveys in the Arctic Ocean have shown turbulent diffusivities over the Atlantic Water layer to be generally in the range O(10^{-5}) to O(10^{-6}) m² s⁻¹ (e.g., Fer, 2009; Guthrie et al., 2017; Sirevaag & Fer, 2012). In particular, staircases have been observed when background diffusivities were O(10^{-6}) m² s⁻¹ (e.g., Guthrie et al., 2017; Sirevaag & Fer, 2012) but were absent for values of O(10^{-5}) m² s⁻¹ (Guthrie et al., 2017). However, these diffusivity values inferred from microstructure measurements require processing to ensure smooth gradients for spectral analysis (Sirevaag & Fer, 2012) and involve depth-averaging over several meters in regions where there is not a diffusive-convective staircase (Fer, 2009; Guthrie et al., 2017). The high-resolution time series of interface structure provided by acoustic sensing may prove useful for estimating variations in mixing levels directly at diffusive-convective interfaces. We may use the background diffusivity as an upper bound on turbulent interface diffusivity, since background diffusivities are estimated over regions of weaker stratification. Then, taking interface κ as O($10^{-5} - 10^{-6}$) m² s⁻¹ yields an eddy length scale of ~ 1 cm for the values of stratification estimated here. Further investigation is needed to determine the appropriate length scales of turbulent overturns that may operate at diffusive-convective interfaces.

4. Summary and Discussion

The continuous and high-resolution echo sounder data allow an unprecedented view of the evolution and persistence of staircase features across the Arctic Ocean. We have analyzed acoustic observations from a broadband echo sounder in the Eurasian Basin. Individual interfaces are tracked in diffusive-convective staircases, and the associated reflection coefficients are related to interface thickness, interface stratification, and turbulent diffusivity. This new methodology may be elucidating in the way diffusive-convective staircases in the Arctic are studied, which has previously relied on labor-intensive microstructure casts, or lower-resolution ITP profiles.

The high-resolution capabilities of the echo sounder in resolving interfaces allow for further insight into how diffusive-convective heat fluxes may vary in space/time. Molecular heat fluxes across interfaces are quantified by $F_H = \rho c_p \kappa_T \partial T / \partial z$, where c_p is the specific heat capacity. Molecular heat fluxes inferred from acoustic data (relating Γ_{Ac} to the temperature gradient via Equation 5) are O(0.1) W m⁻², in agreement with past studies from ITP and microstructure data (e.g., Guthrie et al., 2015; Padman & Dillon, 1987; Shibley et al., 2017).

However, while microstructure or ITP data may be used to provide a single estimate of heat fluxes at a particular time, acoustic data indicate that interface thicknesses, and inferred molecular fluxes, may actually vary by a factor of 2 over just a few hours. The application of turbulent diffusivities, rather than molecular, is likely to modify this result. However, it is not clear for what percentage of time an interface may be turbulent. To yield realistic magnitudes of heat flux of $O(0.1\text{--}1) \text{ W m}^{-2}$ from our estimates of κ , an interface may be affected by localized shear only $\sim 1\%$ of the time, indicating that interfaces may be generally in a molecular, rather than turbulent, state.

Several limitations of acoustic imaging remain to be improved. While the high-frequency capabilities of the echo sounder allow high-resolution imaging of the staircase, they also limit the depth range that can be imaged before signal attenuation (e.g., Ruddick et al., 2009). However, a higher-frequency echo sounder with a larger bandwidth would be better for resolving interface thicknesses. Data from the 15–25 kHz echo sounder may resolve interfaces of $O(10) \text{ cm}$ thick, while an echo sounder with a bandwidth of $O(100) \text{ kHz}$ would be able to resolve interfaces as thin as $O(1) \text{ cm}$, based on the vertical range resolution. This may prove necessary in the Canadian Basin, where interface thicknesses inferred from microstructure measurements can be as thin as $\sim 10 \text{ cm}$ (Timmermans et al., 2008). Finally, our approximations rely on the assumption that the interface density ratio does not change and are then most useful for staircases in steady state.

Echo sounder observations of the ocean are relatively new, and the ability to image turbulence in a warming Arctic Ocean will provide vital insight into how warmer waters can be mixed to the surface. The acoustic methodology presented here may be used across the Arctic to survey staircase properties and relate them to intermittent turbulence affecting diffusive-convective finestructure. A pan-Arctic echo sounder survey with interspersed CTD casts for calibration of sound speed and density ratio could be used to identify regions where staircases are present and to compare to levels of mixing. Further, a continuous survey with a longer time series would allow for an analysis of the Garrett-Munk spectrum, which can then be related to mixing caused by internal waves (Fortin et al., 2016, 2017; Holbrook & Fer, 2005; Holbrook et al., 2003). Future work will involve testing this methodology in the Arctic Ocean and comparing with associated microstructure measurements to investigate levels of mixing.

Data Availability Statement

Data are available in Shibley et al. (2020) at the Bolin Centre for Climate Research Database.

Acknowledgments

Nicole Shibley was supported by the Department of Defense through the National Defense Science and Engineering Graduate Fellowship Program. Christian Stranne received support from the Swedish Research Council (Vetenskapsrådet, 2018-04350). Mary-Louise Timmermans acknowledges funding from the National Science Foundation Office of Polar Programs under Award 1950077.

References

- Carmack, E., Polyakov, I., Padman, L., Fer, I., Hunke, E., Hutchings, J., et al. (2015). Toward quantifying the increasing role of oceanic heat in sea ice loss in the new Arctic. *Bulletin of the American Meteorological Society*, 96(12), 2079–2105. <https://doi.org/10.1175/bams-d-13-00177.1>
- Carpenter, J., Sommer, T., & Wüest, A. (2012). Stability of a double-diffusive interface in the diffusive convection regime. *Journal of Physical Oceanography*, 42(5), 840–854. <https://doi.org/10.1175/JPO-D-11-0118.1>
- Chanona, M., Waterman, S., & Gratton, Y. (2018). Variability of internal wave-driven mixing and stratification in Canadian Arctic shelf and shelf-slope waters. *Journal of Geophysical Research: Oceans*, 123, 9178–9195. <https://doi.org/10.1029/2018JC014342>
- D'Asaro, E. A., & Morison, J. H. (1992). Internal waves and mixing in the Arctic Ocean. *Deep Sea Research Part A. Oceanographic Research Papers*, 39(2, Part 1), S459–S484. [https://doi.org/10.1016/S0198-0149\(06\)80016-6](https://doi.org/10.1016/S0198-0149(06)80016-6)
- Dillon, T. M. (1982). Vertical overturns: A comparison of Thorpe and Ozmidov length scales. *Journal of Geophysical Research*, 87(C12), 9601–9613. <https://doi.org/10.1029/JC087iC12p09601>
- Fer, I. (2009). Weak vertical diffusion allows maintenance of cold halocline in the central Arctic. *Atmospheric and Oceanic Science Letters*, 2(3), 148–152. <https://doi.org/10.1080/16742834.2009.11446789>
- Fer, I., Skogseth, R., & Geyer, F. (2010). Internal waves and mixing in the marginal ice zone near the Yermak Plateau. *Journal of Physical Oceanography*, 40(7), 1613–1630. <https://doi.org/10.1175/2010JPO4371.1>
- Flanagan, J. D., Lefler, A. S., & Radko, T. (2013). Heat transport through diffusive interfaces. *Geophysical Research Letters*, 40, 2466–2470. <https://doi.org/10.1002/grl.50440>
- Fortin, W. F., Holbrook, W. S., & Schmitt, R. W. (2016). Mapping turbulent diffusivity associated with oceanic lee waves offshore Costa Rica. *Ocean Science*, 12(2), 601–612. <https://doi.org/10.5194/os-12-601-2016>
- Fortin, W. F., Holbrook, W. S., & Schmitt, R. W. (2017). Seismic estimates of turbulent diffusivity and evidence of nonlinear internal wave forcing by geometric resonance in the South China Sea. *Journal of Geophysical Research: Oceans*, 122, 8063–8078. <https://doi.org/10.1002/2017JC012690>
- Galbraith, P. S., & Kelley, D. E. (1996). Identifying overturns in CTD profiles. *Journal of Atmospheric and Oceanic Technology*, 13(3), 688–702. [https://doi.org/10.1175/1520-0426\(1996\)013<0688:IOICP>2.0.CO;2](https://doi.org/10.1175/1520-0426(1996)013<0688:IOICP>2.0.CO;2)
- Guthrie, J. D., Fer, I., & Morison, J. (2015). Observational validation of the diffusive convection flux laws in the Amundsen Basin, Arctic Ocean. *Journal of Geophysical Research: Oceans*, 120, 7880–7896. <https://doi.org/10.1002/2015JC010884>
- Guthrie, J. D., Fer, I., & Morison, J. H. (2017). Thermohaline staircases in the Amundsen Basin: Possible disruption by shear and mixing. *Journal of Geophysical Research: Oceans*, 122, 7767–7782. <https://doi.org/10.1002/2017JC012993>

- Holbrook, W. S., & Fer, I. (2005). Ocean internal wave spectra inferred from seismic reflection transects. *Geophysical Research Letters*, 32, L15604. <https://doi.org/10.1029/2005GL023733>
- Holbrook, W. S., Fer, I., Schmitt, R. W., Lizarralde, D., Klymak, J. M., Helfrich, L. C., & Kubichek, R. (2013). Estimating oceanic turbulence dissipation from seismic images. *Journal of Atmospheric and Oceanic Technology*, 30(8), 1767–1788. <https://doi.org/10.1175/JTECH-D-12-00140.1>
- Holbrook, W. S., Páramo, P., Pearse, S., & Schmitt, R. W. (2003). Thermohaline fine structure in an oceanographic front from seismic reflection profiling. *Science*, 301(5634), 821–824. <https://doi.org/10.1126/science.1085116>
- Kelley, D. (1987). Interface migration in thermohaline staircases. *Journal of Physical Oceanography*, 17(10), 1633–1639. [https://doi.org/10.1175/1520-0485\(1987\)017<1633:IMITS>2.0.CO;2](https://doi.org/10.1175/1520-0485(1987)017<1633:IMITS>2.0.CO;2)
- Kelley, D. E. (1988). Small-scale turbulence and mixing in the ocean, pp. 481–502. [https://doi.org/10.1016/S0422-9894\(08\)70566-X](https://doi.org/10.1016/S0422-9894(08)70566-X)
- Krishfield, R., Toole, J., Proshutinsky, A., & Timmermans, M. L. (2008). Automated Ice-Tethered Profilers for seawater observations under pack ice in all seasons. *Journal of Atmospheric and Oceanic Technology*, 25(11), 2091–2105. <https://doi.org/10.1175/2008JTECHO587.1>
- Kwok, R., & Untersteiner, N. (2011). The thinning of Arctic sea ice. *Physics Today*, 64(4), 36–41. <https://doi.org/10.1063/1.3580491>
- Lavery, A. C., Chu, D., & Moum, J. N. (2009). Measurements of acoustic scattering from zooplankton and oceanic microstructure using a broadband echosounder. *ICES Journal of Marine Science*, 67(2), 379–394. <https://doi.org/10.1093/icesjms/fsp242>
- Lavery, A. C., Chu, D., & Moum, J. N. (2010). Observations of broadband acoustic backscattering from nonlinear internal waves: Assessing the contribution from microstructure. *IEEE Journal of Oceanic Engineering*, 35(4), 695–709. <https://doi.org/10.1109/JOE.2010.2047814>
- Lavery, A. C., & Ross, T. (2007). Acoustic scattering from double-diffusive microstructure. *The Journal of the Acoustical Society of America*, 122(3), 1449–1462. <https://doi.org/10.1121/1.2764475>
- Lenn, Y. D., Rippeth, T. P., Old, C. P., Bacon, S., Polyakov, I., Ivanov, V., & Hölemann, J. (2011). Intermittent intense turbulent mixing under ice in the Laptev Sea continental shelf. *Journal of Physical Oceanography*, 41(3), 531–547. <https://doi.org/10.1175/2010JPO4425.1>
- Linden, P., & Shirtcliffe, T. (1978). The diffusive interface in double-diffusive convection. *Journal of Fluid Mechanics*, 87(03), 417–432. <https://doi.org/10.1017/S002211207800169X>
- Lurton, X. (2002). *An introduction to underwater acoustics—Principles and applications*. Chichester, UK: Praxis Publishing.
- Maykut, G. A., & Untersteiner, N. (1971). Some results from a time-dependent thermodynamic model of sea ice. *Journal of Geophysical Research*, 76(6), 1550–1575. <https://doi.org/10.1029/JC076i006p01550>
- Nakamura, Y., Noguchi, T., Tsuji, T., Itoh, S., Niino, H., & Matsuoka, T. (2006). Simultaneous seismic reflection and physical oceanographic observations of oceanic fine structure in the Kuroshio extension front. *Geophysical Research Letters*, 33, L23605. <https://doi.org/10.1029/2006GL027437>
- Neal, V. T., Neshyba, S., & Denner, W. (1969). Thermal stratification in the Arctic Ocean. *Science*, 166(3903), 373–374. <https://doi.org/10.1126/science.166.3903.373>
- Padman, L., & Dillon, T. M. (1987). Vertical heat fluxes through the Beaufort Sea thermohaline staircase. *Journal of Geophysical Research*, 92(C10), 10,799–10,806. <https://doi.org/10.1029/JC092iC10p10799>
- Polyakov, I. V., Pnyushkov, A. V., Alkire, M. B., Ashik, I. M., Baumann, T. M., Carmack, E. C., et al. (2017). Greater role for Atlantic inflows on sea-ice loss in the Eurasian Basin of the Arctic Ocean. *Science*, 356(6335), 285–291. <https://doi.org/10.1126/science.aai8204>
- Polyakov, I. V., Pnyushkov, A. V., Rember, R., Ivanov, V. V., Lenn, Y. D., Padman, L., & Carmack, E. C. (2012). Mooring-based observations of double-diffusive staircases over the Laptev Sea Slope*. *Journal of Physical Oceanography*, 42, 95–109. <https://doi.org/10.1175/2011JPO4606.1>
- Radko, T. (2007). Mechanics of merging events for a series of layers in a stratified turbulent fluid. *Journal of Fluid Mechanics*, 577, 251–273. <https://doi.org/10.1017/S0022112007004703>
- Radko, T. (2013). *Double-diffusive convection*. Cambridge, UK: Cambridge University Press.
- Radko, T., Flanagan, J., Stellmach, S., & Timmermans, M. L. (2014). Double-diffusive recipes. Part II: Layer-merging events. *Journal of Physical Oceanography*, 44(5), 1285–1305. <https://doi.org/10.1175/JPO-D-13-0156.1>
- Rippeth, T. P., Lincoln, B. J., Lenn, Y. D., Green, J. M., Sundfjord, A., & Bacon, S. (2015). Tide-mediated warming of Arctic halocline by Atlantic heat fluxes over rough topography. *Nature Geoscience*, 8(3), 191–194. <https://doi.org/10.1038/NGEO2350>
- Ross, T., & Lueck, R. (2003). Sound scattering from oceanic turbulence. *Geophysical Research Letters*, 30(6), 1343. <https://doi.org/10.1029/2002GL016733>
- Ruddick, B., Song, H., Dong, C., & Pinheiro, L. (2009). Water column seismic images as maps of temperature gradient. *Oceanography*, 22(1), 192–205.
- Schmitt, R. W. (1994). Double diffusion in oceanography. *Annual Review of Fluid Mechanics*, 26, 255–285. <https://doi.org/10.1146/annurev.fl.26.010194.001351>
- Shibley, N. C., & Timmermans, M. L. (2019). The formation of double-diffusive layers in a weakly turbulent environment. *Journal of Geophysical Research: Oceans*, 124, 1445–1458. <https://doi.org/10.1029/2018JC014625>
- Shibley, N. C., Timmermans, M. L., Carpenter, J. R., & Toole, J. M. (2017). Spatial variability of the Arctic Ocean's double-diffusive staircase. *Journal of Geophysical Research: Oceans*, 122, 980–994. <https://doi.org/10.1002/2016JC012419>
- Shibley, N. C., Timmermans, M. L., & Stranne, C. (2020). <https://doi.org/10.17043/shibley-2020>
- Sirevaag, A., & Fer, I. (2012). Vertical heat transfer in the Arctic Ocean: The role of double-diffusive mixing. *Journal of Geophysical Research*, 117, C07010. <https://doi.org/10.1029/2012JC007910>
- Stranne, C., Mayer, L., Jakobsson, M., Weidner, E., Jerram, K., Weber, T. C., et al. (2018). Acoustic mapping of mixed layer depth. *Ocean Science*, 14(3), 503–514. <https://doi.org/10.5194/os-14-503-2018>
- Stranne, C., Mayer, L., Weber, T., Ruddick, B., Jakobsson, M., Jerram, K., et al. (2017). Acoustic mapping of thermohaline staircases in the Arctic Ocean. *Nature: Scientific Reports*, 7(1), 15192. <https://doi.org/10.1038/s41598-017-15486-3>
- Thorpe, S. A. (1977). Turbulence and mixing in a Scottish Loch. *Philosophical Transactions of the Royal Society of London A: Mathematical, Physical, and Engineering Sciences*, 286(1334), 125–181. <https://doi.org/10.1098/rsta.1977.0112>
- Timmermans, M. L., Toole, J., Krishfield, R., & Winsor, P. (2008). Ice-Tethered Profiler observations of the double-diffusive staircase in the Canada Basin thermocline. *Journal of Geophysical Research*, 113, C00A02. <https://doi.org/10.1029/2008JC004829>
- Toole, J. M., Timmermans, M. L., Perovich, D. K., Krishfield, R. A., Proshutinsky, A., & Richter-Menge, J. A. (2010). Influences of the ocean surface mixed layer and thermohaline stratification on Arctic Sea ice in the central Canada Basin. *Journal of Geophysical Research*, 115, C10018. <https://doi.org/10.1029/2009JC005660>
- Turner, J. (1965). The coupled turbulent transports of salt and heat across a sharp density interface. *International Journal of Heat and Mass Transfer*, 8(5), 759–767. [https://doi.org/10.1016/0017-9310\(65\)90022-0](https://doi.org/10.1016/0017-9310(65)90022-0)

- Turner, J. (1968). The behaviour of a stable salinity gradient heated from below. *Journal of Fluid Mechanics*, 33(1), 183–200. <https://doi.org/10.1017/S0022112068002442>
- Wilson, W. D. (1959). Speed of sound in distilled water as a function of temperature and pressure. *The Journal of the Acoustical Society of America*, 31(8), 1067–1072. <https://doi.org/10.1121/1.1907828>
- Wilson, W. D. (1960). Speed of sound in sea water as a function of temperature, pressure, and salinity. *The Journal of the Acoustical Society of America*, 32(6), 641–644. <https://doi.org/10.1121/1.1908167>